Monthly Notices
of the
ROYAL ASTRONOMICAL SOCIETY

MNRAS **461,** 4013–4021 (2016)
Advance Access publication 2016 June 26

doi:10.1093/mnras/stw1524

The sparkling Universe: a scenario for cosmic void motions

Laura Ceccarelli,* Andrés N. Ruiz, Marcelo Lares, Dante J. Paz, Victoria E. Maldonado, Heliana E. Luparello and Diego Garcia Lambas

Instituto de Astronomía Teórica y Experimental (IATE), CONICET-UNC and Observatorio Astronómico, Universidad Nacional de Córdoba, Córdoba X5000BGR, Argentina

Accepted 2016 June 22. Received 2016 June 22; in original form 2015 November 19

ABSTRACT

Cosmic voids are prominent features of the Universe, encoding relevant information of the growth and evolution of structure through their dynamics. Here, we perform a statistical study of the global motion of cosmic voids using both a numerical simulation and observational data. Their relation to large-scale mass flows and the physical effects that drive those motions. We analyse the bulk motions of voids, finding void mean bulk velocities in the range 300–400 km s^{-1}, depending on void size and the large-scale environment. Statistically, small voids move faster, and voids in relatively higher density environments have higher bulk velocities. Also, we find large-scale overdensities (underdensities) along (opposite to) the void motion direction, suggesting that void motions respond to a pull–push mechanism. Our analysis suggests that their relative motions are generated by large-scale density fluctuations. In agreement with linear theory, voids embedded in low (high) density regions mutually recede (attract) each other, providing the general mechanism to understand the bimodal behaviour of void motions. We have also inferred void motions in the Sloan Digital Sky Survey using linear theory, finding that their estimated motions are in qualitatively agreement with the results of the simulation. Our results suggest a scenario of galaxies and galaxy systems flowing away from void centres with the additional, and more relevant, contribution of the void bulk motion to the total velocity.

Key words: methods: data analysis – methods: statistical – cosmology: observations – large-scale structure of Universe.

1 INTRODUCTION

The large-scale flows in the Universe are directly related to the large mass fluctuations associated with the inhomogeneous galaxy distribution (Peebles 1980). This distribution is dominated by large virialized clusters connected by filaments and unveils the presence of large-scale underdense regions widely known as cosmic voids.

This large-scale, underdense regions in the galaxy distribution are also present in dark matter and halo distributions (see, e.g. Bertschinger 1985; Hoyle & Vogeley 2004; Sheth & van de Weygaert 2004; Ceccarelli et al. 2006; Aragon-Calvo et al. 2010; Sutter et al. 2012, and references therein). Based on the fact that dark matter haloes trace the galaxy distribution, Padilla, Ceccarelli & Lambas (2005) have studied and compared voids defined by dark matter, haloes and galaxies, finding that these different tracers produce voids with similar spatial and dynamical properties.

On the other hand, the distributions of mass and voids are strongly connected (White 1979) and therefore void statistics can provide a simplified way to extract information from the clustering pattern, giving clues on the formation and evolution of the cosmic web. Thus, voids have an active interplay with large-scale flows affecting the formation and evolution of structures in the Universe. These large-scale underdensities exhibit local expansion which in some cases, depending on the large-scale environment (Sheth & van de Weygaert 2004; Paz et al. 2013), can be reverted to collapse at larger scales, generating global convergent or divergent flows.

The peculiar velocity field can be directly related to the mass distribution by applying linear theory (Peebles 1980), a fact that can be used to reconstruct it in the observations (Wang et al. 2009). These large-scale flows can be understood as the result of the process of gravitational instability with overdense (underdense) regions attracting (repelling) material. In order to assess the bulk motion of voids we use linearized velocity field to derive the core and shell void bulk motions as in Lambas et al. (2016, hereafter GL16).

Several works have focused on void properties, their dynamics and spatial properties, but their possible bulk motions have received little attention. Nevertheless, large-scale bulk flows have been analysed using the peculiar velocity field in the nearby Universe (Watkins, Feldman & Hudson 2009; Watkins & Feldman 2015).

In GL16 we studied the pairwise velocity of voids in simulations as well as in observational data finding that voids exhibit non negligible coherent motions in the Universe. Here we present

* E-mail: laura@oac.unc.edu.ar

a complementary study of such global motions, focusing into the details of the statistical properties of void velocities and the causes of the void motions. This paper is organized as follows: in Section 2 we describe the data used which comprises the observational and simulated void catalogues, and we include a brief description of the void finder algorithm. In Section 3 we provide an analysis of void motions in the simulation, where we examine the dependences of void velocity and the effects of density around voids on their movement. We also provide a more detailed analysis of the coherence of the pairwise void velocities introduced in GL16 in Section 3.2. In Section 4 we analyse velocities of voids in SDSS and perform a comparison of observational and theoretical results on void motions. Finally, we discuss our results in Section 5.

2 VOID CATALOGUES

2.1 Data sources: galaxy catalogue and simulation

The observational sample of galaxies used in this work was obtained form a volume complete sample extracted from the Main Galaxy Sample (Strauss et al. 2002) of the Sloan Digital Sky Survey Data Release 7 (SDSS-DR7). This sample is defined by a limiting redshift $z = 0.12$ and a maximum absolute magnitude in the r-band $M_r = -20.3$. The parameters defining this galaxy sample are chosen by requiring to be sufficiently dense to minimize shot noise and provide an accurate identification, and large enough to contain a suitable number of voids to obtain statistically significant results. In order to derive void mean peculiar velocities we adopt the linearized velocity field reconstruction by Wang et al. (2012), who used observed groups of galaxies as mass tracers within the framework of linear theory and apply the linear relation between mass overdensity and peculiar velocity (Wang et al. 2009) to associate peculiar velocities to the SDSS regions occupied by voids.

On the numerical side, we use haloes from an N-body dark matter simulation with 1024^3 particles in a cubic volume of $1\,h^{-1}$Gpc on a side. The cosmological parameters $\Omega_M = 0.279$, $\Omega_\Lambda = 0.721$, $\Omega_b = 0.0462$, $h = 0.7$, $n = 0.972$ and $\sigma_8 = 0.821$ correspond to a Λ Cold Dark Matter (ΛCDM) model in concordance with *WMAP*9 results (Hinshaw et al. 2013). Initial conditions were generated using the public code MUSIC (Hahn & Abel 2011). The evolution of the simulation until $z = 0$ was performed with the public version of GADGET-2 (Springel 2005). The simulation was processed with ROCKSTAR (Behroozi, Wechsler & Wu 2013), identifying 3983 265 dark matter haloes as bound structures with at least 20 particles.

2.2 Void identification

The algorithm applied to identify voids is described in Ruiz et al. (2015), which is a modified version of the procedures presented in Padilla et al. (2005) and Ceccarelli et al. (2006). The void finding algorithm selects underdense regions as void candidates, the larger spherical region centred in a void candidate position satisfying $\Delta(R_{\rm void}) < -0.9$ is selected as an underdense sphere, being Δ the integrated density contrast and $R_{\rm void}$ the void radius. Of all underdense spheres selected, the larger ones which do not overlap with any other are identified as voids.

We apply our void finding algorithm to the haloes in the numerical simulation and to the volume limited sample of galaxies. The final void catalogues contain 13 430 voids in the halo distribution and 363 galaxy voids. We notice that Wang et al. (2012) conclude that the bias in the reconstruction of the SDSS peculiar velocity field is small in the inner region of the survey. The volume for which this field is reliably determined by this method is approximately two thirds of the total volume of the main galaxy sample. Consequently, we have considered 245 voids, identified in the observational data restricted to this smaller region.

3 THE MOTION OF VOIDS

Void internal dynamics is characterized by a bimodal behaviour which strongly depends on the large-scale environment (Sheth & van de Weygaert 2004; Paz et al. 2013). Although the central regions of all voids show similar dynamics consistent with radial expansion, the surrounding mass distribution determines the velocity field at void shells, making voids dynamically connected to the cosmic web (Ruiz et al. 2015).

It has been widely assumed that voids are at relative rest with respect to the comoving coordinate system, however this topic has not been analysed in detail. The motions of voids as full entities have been noticed by Gottlöber et al. (2003), although on the other hand, it has been suggested that voids may have negligible bulk velocities (Sutter et al. 2014). We notice that it is difficult to compare possibly contradictory results on a common basis due to the different type of void identification schemes involved. Void bulk velocities are influenced by large-scale density contrasts, so that voids identified with different underdensity thresholds could have different velocities. Recently, Wojtak, Powell & Abel (2016) have reported void motions using a voidfinder analogue to ZOBOV (Neyrinck 2008). It is worth mentioning that void motions are also detected using different methods. In a recent paper, we have determined the existence of a bimodal behaviour of voids motions (GL16). Inspired on these results, in this work we analyse the dynamics of voids as global entities considering the peculiar velocity field as well as their connection with the large-scale mass distribution. In this section we show that voids are non–static components of the large-scale Universe, exhibiting significant peculiar motions.

3.1 The large-scale environment of voids and its relation to void global motions

Throughout this paper we use the void–shell mean velocity instead of that of void cores. This is suitable since by definition there are very few galaxies (haloes) inside voids and we have shown previously that shell bulk velocities trace well the void core motions (GL16). According to this, to compute the void velocities we calculate the mean bulk velocity of haloes located at void–centric distances between 0.8 and 1.2 void radius, which correspond to the denser shell surrounding voids.

Panel (a) of Fig. 1 shows the mean void velocities as a function of void radius in the simulation. Black circles show the complete sample of simulated voids, the error bars represent the error of the mean and the region enclosed by the grey solid lines indicates the velocity dispersion. It can be seen in this figure a clear trend of smaller velocities for large voids, smaller ones ($R_{\rm void} < 10\,h^{-1}$ Mpc) exhibiting velocities as large as 400 km s^{-1}, decreasing to 300 km s^{-1} for the largest voids. The black solid line in the figure indicates the mean velocity of randomly placed shells in the simulation box. It can be noticed that the motions of voids and randomly placed shells are similar, showing that voids are equally affected by the large-scale flows originated by the large-scale structure. Taking into account that the sources of peculiar velocities are mass density fluctuations and the presence of large-scale mass correlations, we have compared the motion of voids embedded in different global density environments. For this purpose, we have analysed the dependence of void

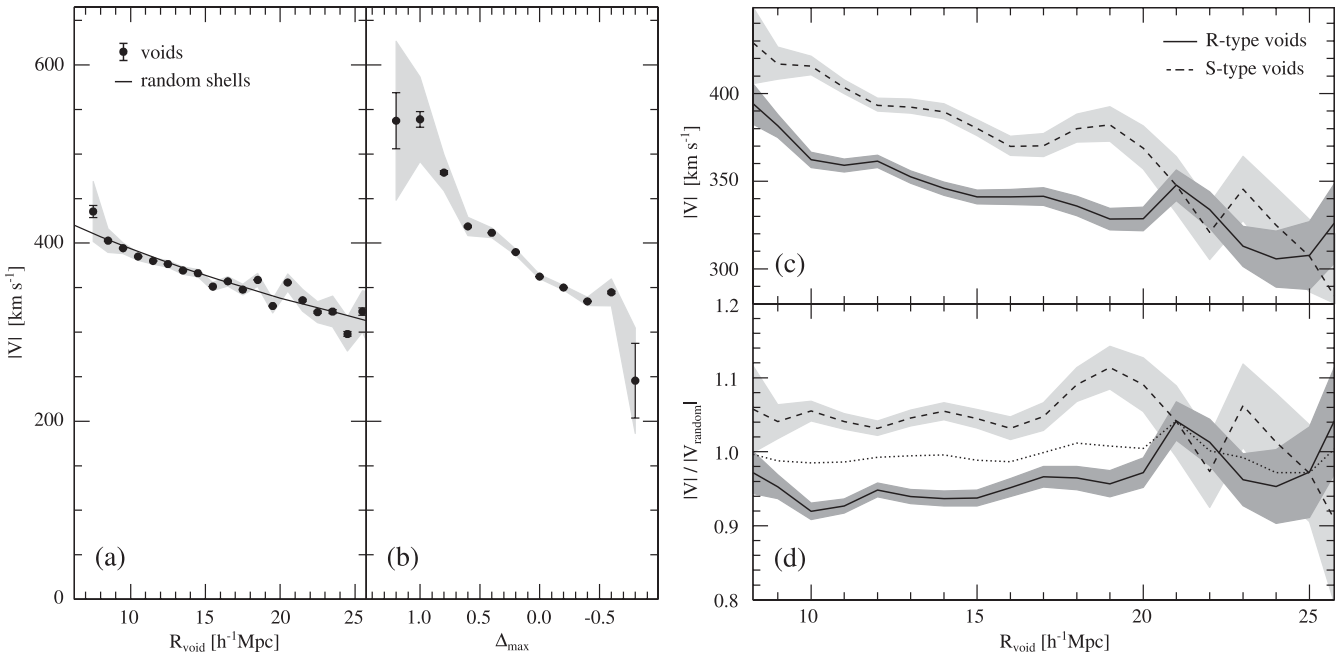

Figure 1. Left: in panel (a) we show the mean velocity for voids in the simulation box as a function of void radii (black points). The solid black line indicates the mean velocity of randomly centred spheres. Panel (b) shows the mean velocity of voids as a function of Δ_{max} (black points). In both panels the error bars indicate the standard error on the mean velocity and the grey regions shows the standard deviation of the velocity distribution. Right: in panel (c) we show the mean velocity as a function of the void radius for S-type (dashed line) and R-type voids (solid line) in the simulation. Panel (d) shows the ratio between the mean velocities of void and random spheres as a function of size for the full void sample (dotted line), S-type voids (dashed line) and R-type voids (solid line) in the simulation. The grey shaded regions represent the standard deviation of the velocity distributions in both panels.

bulk velocities on the surrounding large-scale density of haloes. In panel (b) of Fig. 1 we show the void mean velocity as a function of maximum overdensity at void environment (Δ_{max}) which, for each void, is the absolute maximum of the integrated density profile at distances between 2 and 3 R_{void} to the void centre (see Ceccarelli et al. (2013) for a more detailed explanation of Δ_{max}). As it can be seen in the figure, void mean velocities show a positive trend, ranging approximately 300 km s^{-1} for voids with $\Delta_{max} \sim -0.5$ to velocities higher than 500 km s^{-1} for voids with $\Delta_{max} > 1.0$.

In order to disentangle the effects of void environment and size on velocities, we have also analysed the velocity dependence on void radius for voids in low and high density regions, namely R- and S-type voids, separately (Ceccarelli et al. 2013; Paz et al. 2013). We notice that our void classification is actually based on the close void environment, where R-type voids are surrounded by underdense large-scale regions ($\Delta_{max} < 0$) and S-type voids corresponds to voids embedded in overdense regions ($\Delta_{max} > 0$). This classification is closely related to void evolution and describes in a simple way the two different modes, namely the void–in–void and void–in–cloud processes (Sheth & van de Weygaert 2004). Motivated by these classical results, we have analysed void evolution adopting a criterion based on the density around voids, to select voids in overdense and underdense regions (S-type and R-type voids respectively) in order to associate them with the void-in-void and void-in-cloud pictures.

Given the large differences of the dynamics of shells surrounding voids embedded in low and high density regions (Ruiz et al. 2015) we can also envisage to find differences of void bulk velocities of the two void types. The mean bulk velocities are shown in panel (c) of Fig. 1, where the dashed lines indicate the mean for S-type voids and the solid lines correspond to the mean for R-type voids, the regions between grey lines indicate the 1σ deviations of the mean. We show the results for void radii in the range 10–25 h^{-1} Mpc, suitable to compare the velocity of both types of voids with statistically significant number of voids. We notice that we obtain systematic larger mean velocities for S-type voids and reach the highest values for small S-type voids, $\sim$400 km s^{-1} for $R_{void} < 12\,h^{-1}$ Mpc. Large R-type voids have mean bulk velocities below 350 km s^{-1}. Besides the statistical dependence of void size on the surrounding density, the magnitude of mean void velocity is related to both, void size and environment. This behaviour could be a natural outcome of the stronger gravitational pull of the dense regions surrounding S-type voids (as it will be seen in the discussion of Fig. 3 below).

We have also compared the mean bulk velocity of voids in different large-scale environments with that of randomly placed spheres. For both voids and random spheres, the bulk velocity is obtained by calculating the mean velocity of dark matter haloes in shells of radius R_{void}. The ratio of void/random sphere velocities as a function of void size are displayed in panel (d) of Fig. 1, for R-type voids (solid line), S-type voids (dashed line) and the full sample of voids (dotted line). As it is can be appreciated in this figure, randomly placed spheres velocities show an intermediate behaviour between S-type and R-type voids. Since the random spheres sample should comprise a mixture of overdense and underdense regions, it is expected an intermediate behaviour between the overdense and underdense void shells.

In Fig. 2 we display the magnitude of the void velocity distributions for S- and R-type voids where it can be seen that their velocities span a wide range of values, ranging from 0 to 1000 km s^{-1}. By a more detailed inspection, it can be noticed that S-type voids tend to have velocities systematically larger than R-type voids, with an excess of voids with velocities larger than 800 km s^{-1}, and up to 1000 km s^{-1} for S-type voids (dashed line), whereas R-type voids remain mostly below 800 km s^{-1} (solid line). Vertical lines in Fig. 2

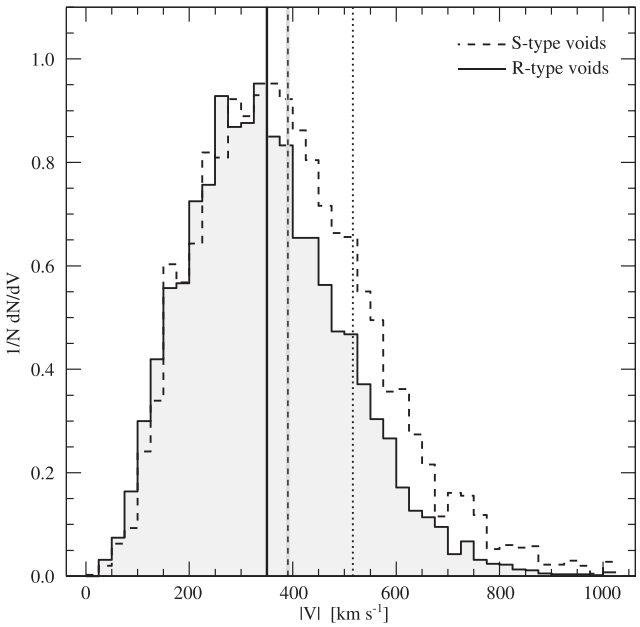

Figure 2. Void velocity normalized distributions for the voids identified in the numerical simulation. S-type voids are represented with the dashed line and R-type voids with the solid line. Vertical solid (dashed) line shows the mean velocity value for R-type (S-type) voids. Shaded bands around these lines represent the standard error of the mean values. Vertical dotted line indicates the mean velocity of haloes having $M > 10^{12}\,h^{-1}\,\mathrm{M}_{\odot}$.

show the mean void velocity for S-types (dashed) and R-types (solid), corresponding to 390 km s^{-1} and 350 km s^{-1}, respectively. Grey shaded bands represent the error of the mean. The dotted vertical line at 515 km s^{-1} show the mean velocity of dark matter haloes. We have selected the haloes having $M > 10^{12}\,h^{-1}\,\mathrm{M}_{\odot}$ in the simulation box and we calculate their averaged velocity obtaining a mean of 515 km s^{-1}, which is consistent with those obtained by Pivato, Padilla & Lambas (2006). It is remarkable that mean void and halo velocities are of the same order despite their very different nature, haloes being the most compact, extremely dense objects, and voids the largest empty regions in the Universe.

In order to shed light on the sources of the motion of voids we have explored the relation between the direction of bulk motion and the mass density distribution surrounding voids. For this aim, we have stacked the mass density distribution surrounding voids aligning with the velocity vector and normalizing the distances to void radii. The resulting stacking has axial symmetry with respect to the void velocity vector and so we average the signal around this direction. In Fig. 3 we show the normalized density maps of stacked voids where the y-axis direction correspond to that of voids bulk motion. In panel (a) we display the results for S-type voids, and in panel (b) for R-type voids. Both subsamples have $10 < R_{\rm void}/\,h^{-1}$ Mpc < 14, a range selected in order to have enough number of R- and S-type to enhance visualization, although the same pattern occurs for different size ranges. The normalized density contrast (δ) increases from blue to red and white colour corresponds to the mean density, as it is indicated in the colour bar. It can be seen that for both void types the motion points towards overdensities, being larger for the case of S-type voids. This is expected due to the definition of S-type voids, which are embedded in regions with higher densities ($\Delta_{\rm max} > 0$). We also notice that void are pushed away from underdense regions as expected if voids follow the global flow pattern driven by large-scale mass fluctuations. In this case, R-type voids present

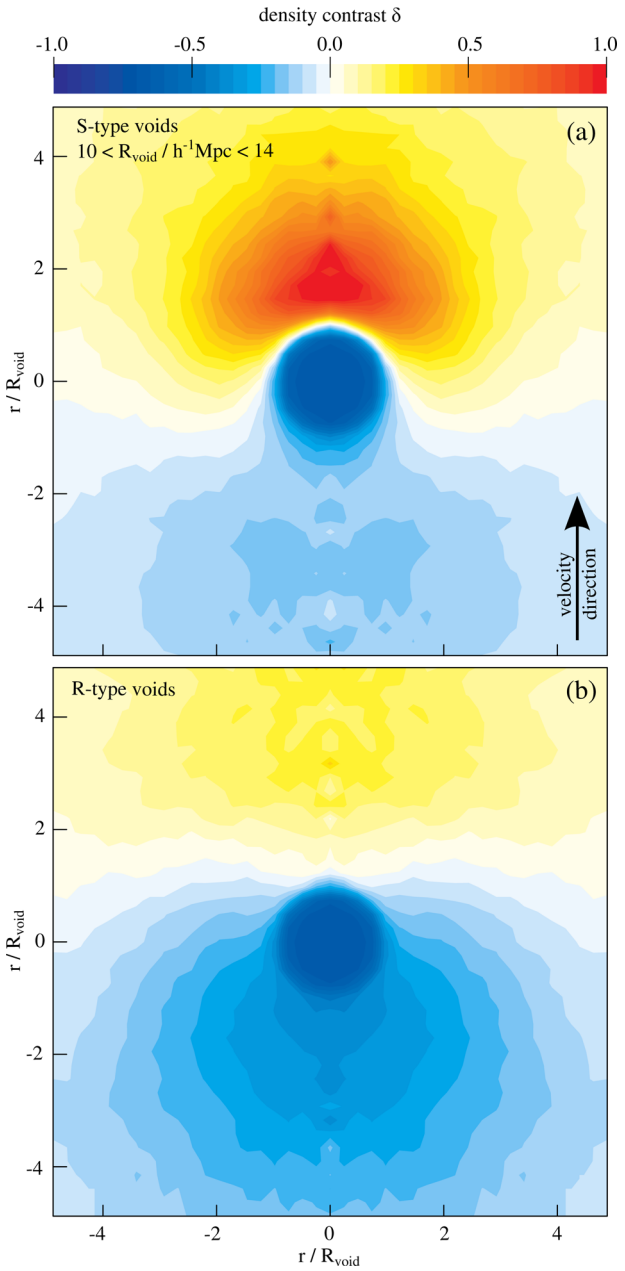

Figure 3. Normalized stacked density contrast (δ) around S-type (panel (a)) and R-type (panel (b)) voids in simulation for sizes in the range $10 < R_{\rm void}/\,h^{-1}$ Mpc < 14. Distances are normalized to void sizes and y-axis is aligned to void velocity direction. Colour bar in the top shows the value of the normalized stacked δ.

a more noticeable underdensity opposite to the direction of void motions. The general picture of void motions can be understood in terms of a pull and push mechanism driven by the large-scale velocity flows, where S-type voids in high density environments are pulled by the collapsing structures and R-type voids are pushed away from the expanding underdense environment in which they are embedded.

3.2 Coherence of pairwise large-scale void motions

In GL16 we reported two void populations according to their large-scale environment: voids mutually receding and those mutually

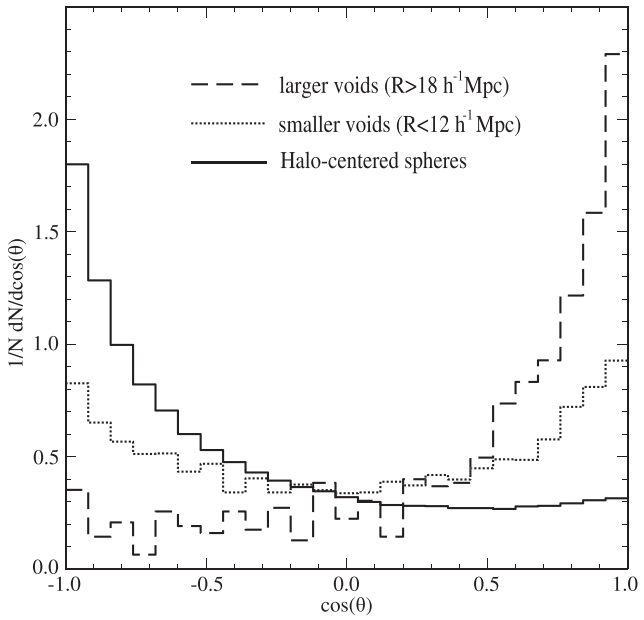

Figure 4. Number counts of pairs of spheres having velocities with relative orientations given by $\cos(\theta)$. The dashed line corresponds to large voids in the void catalogue ($R_{\rm void} > 18\,h^{-1}$ Mpc), the dotted line corresponds to the small voids ($R_{\rm void} < 12\,h^{-1}$ Mpc) and the solid line corresponds to spheres around high mass haloes ($M > 10^{14}\,h^{-1}\,{\rm M}_{\odot}$), with the same size distribution than that of the void sample.

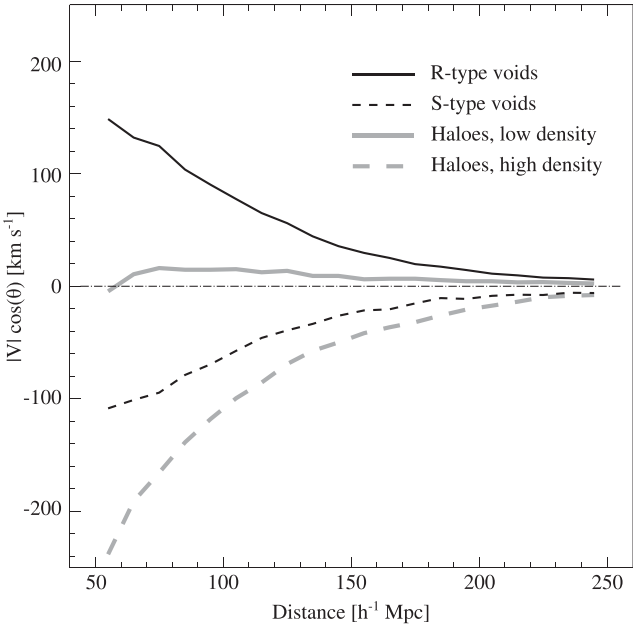

Figure 5. Pairwise velocity ($|V|\cos(\theta)$) of spheres of radius R as a function of the relative separation in the simulation. The solid and dashed black lines correspond to R-type and S-type void pairs, respectively. The solid (dashed) grey lines correspond to spheres centred on haloes with $M > 10^{14}\,h^{-1}$ Mpc, with a total integrated density up to $3R$ lower (greater) than the mean, following the similar procedure as in voids. The sphere radius R was taken at random from the same distribution of void radii.

approaching. In this work, it was also analysed the connection between the pairwise motion bimodality and void classification, finding S-type void pairs systematically approaching each other, and R-type voids mutually receding.

Upcoming surveys such as Hobby–Eberly Telescope Dark Energy Experiment (HETDEX, Hill et al. 2008), Euclid (Amendola et al. 2013) or Dark Energy Spectroscopic Instrument (DESI, Eisenstein & DESI Collaboration 2015) can lead to a revolutionary progress on observational cosmology, since they will cover unprecedented large scales, thus providing more significant samples of large voids. In previous works (see, for instance, Ceccarelli et al. 2013), we notice that the largest voids which are those most likely to be involved in several cosmological tests, are of R-type and therefore are expected to have systematically mutually receding motions, contrasting to the bimodal behaviour of a mixed population of void types (GL16). It is expected that this behaviour could be seen through the distributions of $\cos(\theta)$ values, being θ the angle between the difference velocity vector and the vector separation between voids as shown in Fig. 4, where dashed lines and dot–dashed lines correspond to large and small voids, respectively. Note that in this scheme positive (negative) values of $\cos\theta$ indicate mutually receding (approaching) voids. Then, large voids, which are likely R-type, tend to recede and smaller voids, which are a mixture of R and S-types, show a bimodal distribution of approaching and receding voids. For a suitable comparison, we also analysed regions centred in the most massive haloes ($M > 10^{14}\,h^{-1}\,{\rm M}_{\odot}$), considering that these systems will tend to be embedded in large overdense environments. As it is shown in solid lines in Fig. 4, shells centred in massive haloes corresponding to clusters of galaxies are likely to be approaching each other, similarly to S-type voids, largely contrasting with the opposite behaviour of large, R-type voids mutually receding.

In order to perform a more detailed analysis of the relative motions of voids and to put them within the large-scale context, we have compared the relative pairwise velocity ($|V|\cos(\theta)$) as a function of relative separation for spheres of radius R centred in $M > 10^{14}\,h^{-1}\,{\rm M}_{\odot}$ haloes, constrained to reside in different density environments. The results are shown in Fig. 5 for spheres classified into low and high large-scale density, according to the integrated mass density up to 3 sphere radius similarly to the criterion applied to void classification into S- and R-types. It is worth mentioning that 97 per cent of these haloes are outside $1.2R_{\rm void}$ from any void so that the sample of massive halo–centred spheres trace different regions from that of voids and allows us to analyse void motions in the general context of global flows. As a distinction to voids, which exhibit a bimodal behaviour of approaching and receding motions depending on the large-scale overdensity (Fig. 5, solid lines), spheres centred in the most massive haloes have mainly mutually approaching motions. Also, independently of the constraints in the global surrounding mass density, they do not show mean receding motions, as shown with dashed lines in Fig. 5.

We also acknowledge that the filamentary structure surrounding voids is mostly populated by relatively low mass haloes (Cautun, van de Weygaert & Jones 2013), so their global motion is related to that of the void core (GL16). We have explored this behaviour by studying the correlated pairwise velocities for low and high halo mass ranges, defined by haloes having $M < 10^{14}\,h^{-1}\,{\rm M}_{\odot}$ and $M < 10^{14}\,h^{-1}\,{\rm M}_{\odot}$, respectively. We select haloes in low and high large-scale environment, finding that the low mass haloes exhibit a similar behaviour than voids. Specifically, low mass haloes in low density environments exhibit receding motions, similar to a pair of R-voids, whereas low mass haloes in high density regions attract each other, like S-type voids.

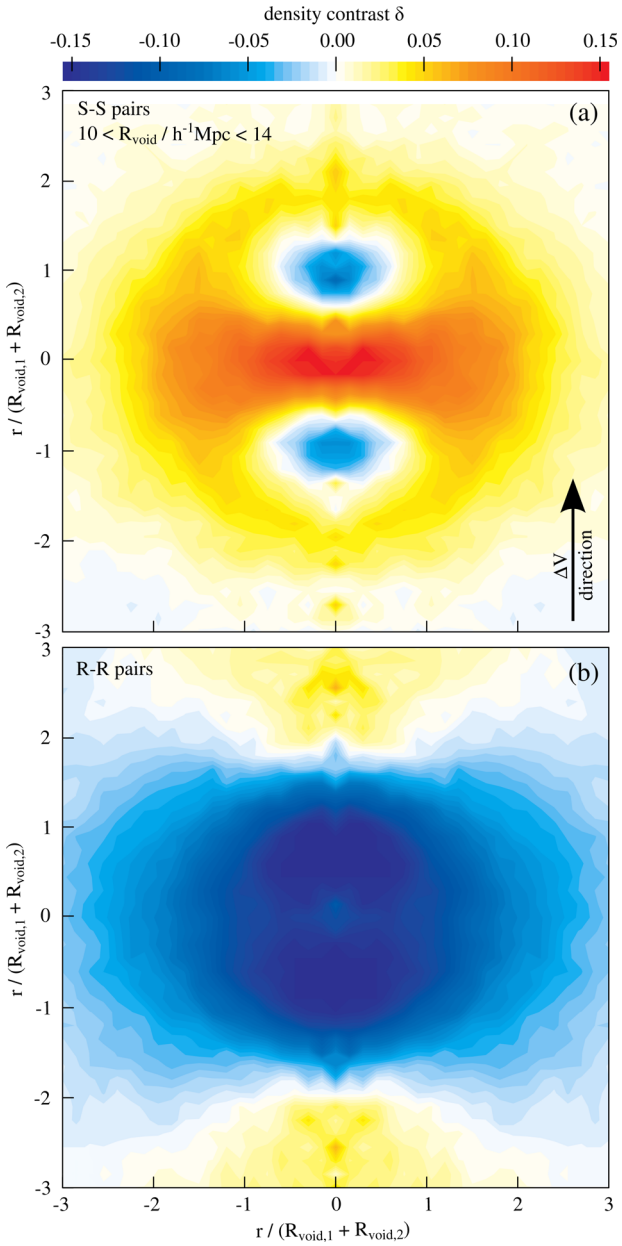

Figure 6. Normalized staked density contrast (δ) for S–S (panel (a)) and R–R void pairs (panel (b)). Void pairs are selected from a subsample with sizes in the range $10 < R_{\rm void}/\,h^{-1}$ Mpc < 14 and a separation between 1.5 and 3 times the sum of their radii. Distances are normalized to the sum of void radii and the y-axis is oriented to the velocity difference direction. As this direction is aligned with the relative separation direction, the coherent patter emerges. Colour bar in the top shows the value of the normalized stacked δ.

In Fig. 6 we show the halo density around void pairs by stacking the pairs aligned to the vector of their relative velocity difference. Panel (a) of Fig. 6 correspond to S–S void pairs, meanwhile R–R pairs are shown in panel (b). In both cases, voids have a separation distance in the range 1.5–3 on units of the sum of the void radii and with sizes from $10\,h^{-1}$ Mpc to $14\,h^{-1}$ Mpc. As in Fig. 3, colours indicate the mass overdensity values of the resulting stacking. It can be noticed that the relative velocity of voids tend to be aligned with the relative separation vector (GL16), for this reason the two bluest regions correspond to the largest underdensities where voids are more likely located.

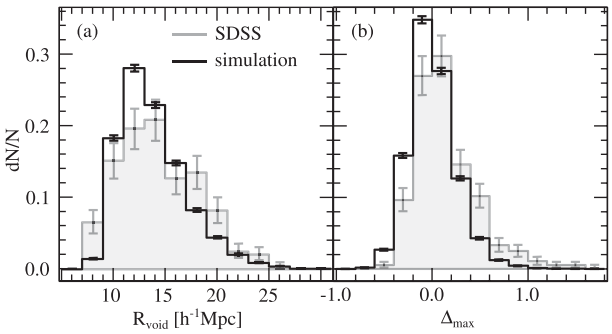

Figure 7. Normalized number counts of voids as a function of void radius ($R_{\rm void}$) in panel (a) and as a function of maximun overdensity ($\Delta_{\rm max}$) in panel (b). In both panels voids identified in the SDSS-DR7 are in grey lines and voids identified in the numerical simulation in black lines. The errorbars for dN/N correspond to Poisson uncertainties.

As it can be seen in the upper panel of Fig. 6, there is a noticeable overdensity between S-type void pairs. Consistent with mass fluctuation governing the peculiar velocity field, this figure shows how the approaching motion of S-type void pairs found in GL16 is driven by this overdense region residing typically along the direction of their relative separation. By contrast, the density map of the lower panel of Fig. 6 exhibit an underdense region between voids, and overdensities in the opposite direction. This is consistent with a picture where voids are strongly affected by the global environment, a larger fraction of small voids are likely to be in overdense regions so that two close S-type voids will tend to approach each other due to the action of the overdensity in which they are embedded. On the other hand, a pair of R-type voids, likely residing in a global underdense region, will tend to be moving away from each other, pushed by the underdense region between them, and pulled by denser regions at large distances. These results provide further explanation to the coherence of void motions presented in GL16.

4 THE MOTION OF OBSERVATIONAL VOIDS

Once we have analysed into some detail void motion in the numerical simulation, in this section our aim is to study the motions of observational voids in a similar fashion. To validate a direct comparison between the results obtained in the numerical simulation with those we will present in the following sections for the SDSS-DR7, in Fig. 7 we compare the normalized number counts of voids as a function of void radius (panel (a)) and as a function the maximum overdensity $\Delta_{\rm max}$ (panel (b)). The distributions of voids identified in the SDSS-DR7 and in the numerical simulation are plotted in grey and black lines, respectively. The errorbars for dN/N correspond to Poisson uncertainties. Due to the fact that both populations shares similar distributions of sizes and $\Delta_{\rm max}$, we can expect similar properties of bulk motions in the observational voids than those obtained previously in the numerical simulation.

4.1 Void velocities

In order to assign peculiar velocities to galaxies in the observational sample we adopt the linearized velocity field derived for the SDSS-DR7 region by Wang et al. (2012). Velocities for observational voids are calculated following the same procedure than in the simulation. In GL16 we have shown that velocities of void shells

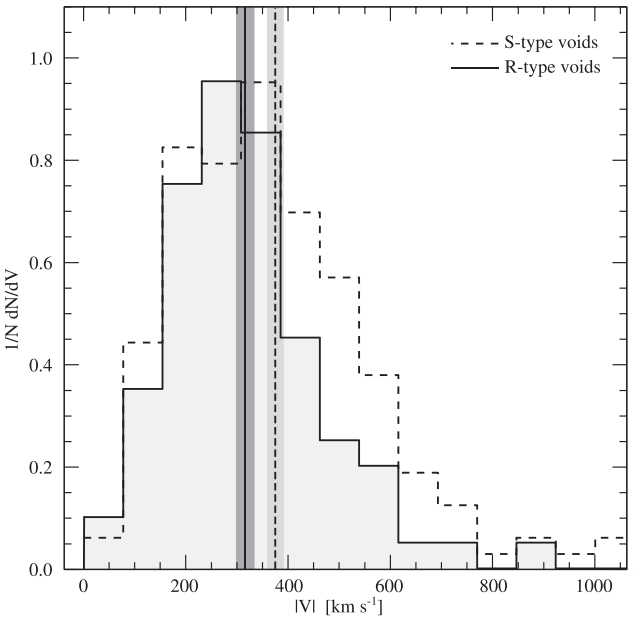

Figure 8. Void velocity normalized distributions for the voids identified in the SDSS data. S-type voids are represented with the dashed line and R-type voids with the solid line. Vertical solid (dashed) line shows the mean velocity value for R-type (S-type) voids. Shaded bands around these lines represent the standard error of the mean values.

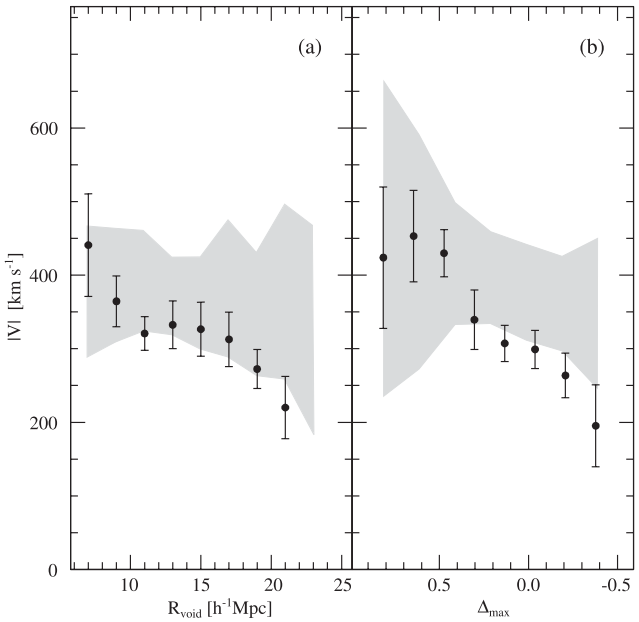

Figure 9. In panel (a) we show the mean bulk velocity of voids in the SDSS as a function of void radii and in panel (b) the same mean bulk velocity as a function of Δ_{max} (black points). In both cases, the error-bars correspond to the standard error of the mean and the grey shaded areas represent an estimation of cosmic variance (see text for details).

in the numerical simulation suitably trace void global motions. The validation of these results for observational data, and a justification of the use of a linearized velocity field are presented in Appendix A.

In Fig. 8 we display the void velocity distribution for S- and R-type voids in SDSS. As it can be seen, the derived void bulk velocity distribution is similar to that corresponding to voids in the simulation (see Fig. 2), ranging from 0 to 1000 km s^{-1} for R- and S-type voids. The same trend observed in the simulation is found here, where S-type voids are more likely to have larger bulk velocities than R-type voids, with an excess of voids with velocities larger than 800 km s^{-1} for S-type voids (dashed line), whereas R-type voids remain mostly below 600 km s^{-1} (solid line). Vertical lines in Fig. 8 indicate the mean void velocity for S-type (grey dashed vertical line) and R-type (black dashed vertical line), corresponding to 370 km s^{-1} and 310 km s^{-1}, respectively. These results are in qualitative agreement with those obtained in numerical simulations (see Fig. 2).

We have also analysed the dependence of void velocity on void size and Δ_{max}. In panel (a) of Fig. 9 we show the mean void velocities as a function of void radius in the SSDS. Black circles show the complete sample of SDSS voids, with error bars representing the error of the mean. The grey shaded region represents an estimation of the cosmic variance effect on the mean void velocities from simulations. We split the simulation box into 64 independent realizations in the simulation with the same volume than that spanned by the SDSS sample. As it can be noticed in this panel, these trends are similar to those obtained in the simulation where velocities become smaller as void size increases, from ∼500 km s^{-1} to ∼200 km s^{-1} for voids with $7 < R_{void}/h^{-1}$ Mpc < 21. In panel (b) of Fig. 9 we show the void mean velocity as a function of maximum overdensity at void environment (Δ_{max}). In this panel it can be seen that the mean velocities show a significant trend, from approximately 200 km s^{-1} for voids with $\Delta_{max} \sim -0.5$ to velocities higher than 400 km s^{-1} for voids with $\Delta_{max} > 1.0$. It can be noticed that mean void velocities in the observations are in good agreement with those predicted by simulations (grey shaded region). We infer that voids in SDSS have significant bulk motions and have dependences on void size and large-scale environment consistent with those found in the simulation. It is important to stress the suitable agreement between theoretical and observational results, in particular, given the limitations of the observational samples.

It is worth to mention that the possibility of using linearized velocity fields to derive void bulk flows allows us to apply the method developed by Wang et al. (2009) to diverse observational samples. This could be a powerful tool to analyse the large-scale flows traced by the void velocities. This could be an interesting opportunity to carry out statistical studies of the dynamic of voids in available galaxy surveys, without limiting to the nearby regions where peculiar velocities can be measured accurately.

5 DISCUSSION AND CONCLUSIONS

In this paper we explore into detail the phenomenology of void motions as presented in GL16. Voids exhibit significant bulk motions and, in general, void and halo velocities follow the large flows induced by large-scale mass fluctuations in the Universe. The interpretation of bulk flows is limited by the effects of small scale motions (Watkins & Feldman 2015). The advantage of analysing the large-scale bulk motions through void motions is due to the simple internal dynamics that allow as to disentangle the local and global velocity fields. In contrast to the case of spheres of the same volume centred in clusters or randomly, void dynamics is governed by a divergent velocity field so that galaxies (or haloes) flowing away from voids are subject to both void shell expansion and bulk motion, indicating that void shells are in relative expansion with respect to the central core region. Moreover, the radial outflow is not strongly turbulent, with comparable albeit smaller, velocity dispersion in the shell surface (Padilla et al. 2005) with respect

to the shell radial velocity. The large bulk velocities of voids in cosmological volumes found in this work imprint a global motion to those of haloes in the shells. In this simple scenario, bulk flows can be thought of as a combination of void (shell) global motions plus radial outflow and dispersion. We notice that void (shell) bulk motions are of comparable magnitude to that of haloes, in particular for those with $M < 10^{14}\,h^{-1}\,\mathrm{M}_{\odot}$). This is not totally surprising since void shells are populated by relatively low-mass haloes so that the bulk velocities of the void shells are a major contribution to halo motions superimposed to the void shell expansion.

Similarly, void pairwise velocities are consistent with that of large-scale systems with motions generated by large-scale density fluctuations. In general, low (high) density regions mutually recede (attract) each other consistent with a basic statement of Newtonian dynamics in an expanding world model. Regions centred in high density peaks show approaching velocities in a similar way than voids embedded in overdense regions. On the contrary, very large, low density regions, are populated by voids in the galaxy/halo distribution, and are characterized by a global expansion. Our results on void pairwise motions, introduced on GL16 and expanded here, provide an alternative description of the evolution of the large-scale structure of the Universe. On this scenario, the coherent and non negligible bulk motions of voids are supposed to play a fundamental role in the formation of structures (Anderson et al. 2014). Voids are affected by relative velocities of $\sim$400 km s^{-1} at very large scales (up to 200 h^{-1} Mpc), these large scale flows should be correlated with significant density fluctuations in regions larger than 100 h^{-1} Mpc (Watkins et al. 2009), which are compatible with the anisotropies on dark matter distribution around voids showed here (as it can be seen in Figs 3 and 6). Such large scale anisotropies in matter distribution could be controversial with predictions derived from Cosmic Microwave Background probes (Kashlinsky et al. 2008; Watkins, Feldman & Hudson 2009; Feldman, Watkins & Hudson 2010; Lavaux et al. 2010; Colin et al. 2011; Ma, Li & He 2015).

Then, having knowledge of the coherence and non-negligible motions of voids is crucial for observational cosmology. For instance, the motion of galaxies and clusters at large scales (Nusser, Branchini & Davis 2011; Turnbull et al. 2012; Ma & Pan 2014; Hoffman, Courtois & Tully 2015) could be governed by the large-scale streaming flows driven by cosmological voids, generating significant bulk velocities at scales around a few hundred h^{-1} Mpc. These motions, and the fluctuations associated with them, are not fully compatible with predictions based on ΛCDM cosmological models.

We also forecast the impact of these results on cosmological tests using voids in forthcoming large-scale surveys such as HETDEX (Hill et al. 2008), Euclid (Amendola et al. 2013) or DESI (Eisenstein & DESI Collaboration 2015). The accurate description of the velocity and density field around voids is critical to properly perform cosmological test like the Alcock–Paczynski (Lavaux & Wandelt 2010; Sutter et al. 2012) or the Integrated Sachs–Wolfe effect (Granett, Neyrinck & Szapudi 2008; Pápai, Szapudi & Granett 2011; Hernández-Monteagudo & Smith 2013; Ilić, Langer & Douspis 2013; Cai et al. 2014), and our results could become relevant on this context contributing to the field by including a possible scenario for large-scale flows based on the concordance cosmological model.

The non–negligible and coherent mutual void bulk motions observed here could contribute to the motion of clusters and galaxies at intermediate densities, in filaments or walls. We stress the fact that bulk velocities of voids in observational data are in concordance with the theoretical results. We also note that the linear approximation used to derive velocities are suitable for the analysis of the bulk motion of voids in the observations (see Appendix A).

ACKNOWLEDGEMENTS

We thank helpful comments and suggestions from the anonymous referee, which have improved and clarified this work. This work has been partially supported by Consejo de Investigaciones Científicas y Técnicas de la República Argentina (CONICET) and the Secretaría de Ciencia y Técnica de la Universidad Nacional de Córdoba (SeCyT). Funding for the SDSS and SDSS-II has been provided by the Alfred P. Sloan Foundation, the Participating Institutions, the National Science Foundation, the U.S. Department of Energy, the National Aeronautics and Space Administration, the Japanese Monbukagakusho, the Max Planck Society, and the Higher Education Funding Council for England. The SDSS web site is http://www.sdss.org/. The SDSS is managed by the Astrophysical Research Consortium for the Participating Institutions. The Participating Institutions are the American Museum of Natural History, Astrophysical Institute Potsdam, University of Basel, University of Cambridge, Case Western Reserve University, University of Chicago, Drexel University, Fermilab, the Institute for Advanced Study, the Japan Participation Group, Johns Hopkins University, the Joint Institute for Nuclear Astrophysics, the Kavli Institute for Particle Astrophysics and Cosmology, the Korean Scientist Group, the Chinese Academy of Sciences (LAMOST), Los Alamos National Laboratory, the Max-Planck-Institute for Astronomy (MPIA), the Max-Planck-Institute for Astrophysics (MPA), New Mexico State University, Ohio State University, University of Pittsburgh, University of Portsmouth, Princeton University, the United States Naval Observatory, and the University of Washington. We thank Dr Mario A. Sgró for kindly providing the numerical simulation and halo catalogue. Some of the plots presented in this work were made by using R software and post processed using INKSCAPE. This research has made use of NASA's Astrophysics Data System.

REFERENCES

Amendola L. et al., 2013, Living Rev. Relativ., 16, 6
Anderson L. et al., 2014, MNRAS, 441, 24
Aragon-Calvo M. A., van de Weygaert R., Araya-Melo P. A., Platen E., Szalay A. S., 2010, MNRAS, 404, L89
Behroozi P. S., Wechsler R. H., Wu H.-Y., 2013, ApJ, 762, 109
Bertschinger E., 1985, ApJS, 58, 1
Cai Y.-C., Neyrinck M. C., Szapudi I., Cole S., Frenk C. S., 2014, ApJ, 786, 110
Cautun M., van de Weygaert R., Jones B. J. T., 2013, MNRAS, 429, 1286
Ceccarelli L., Padilla N. D., Valotto C., Lambas D. G., 2006, MNRAS, 373, 1440
Ceccarelli L., Paz D., Lares M., Padilla N., Lambas D. G., 2013, MNRAS, 434, 1435
Colin J., Mohayaee R., Sarkar S., Shafieloo A., 2011, MNRAS, 414, 264
Eisenstein D., DESI Collaboration, 2015, Am. Astron. Soc. Meeting Abstr., 225, 336.05
Feldman H. A., Watkins R., Hudson M. J., 2010, MNRAS, 407, 2328
Gottlöber S., Łokas E. L., Klypin A., Hoffman Y., 2003, MNRAS, 344, 715
Granett B. R., Neyrinck M. C., Szapudi I., 2008, ApJ, 683, L99
Hahn O., Abel T., 2011, MNRAS, 415, 2101
Hernández-Monteagudo C., Smith R. E., 2013, MNRAS, 435, 1094
Hill G. J. et al., 2008, in Kodama T., Yamada T., Aoki K., eds, ASP Conf. Ser. Vol. 399, Panoramic Views of Galaxy Formation and Evolution. Astron. Soc. Pac., San Francisco, p. 115
Hinshaw G. et al., 2013, ApJS, 208, 19
Hoffman Y., Courtois H. M., Tully R. B., 2015, MNRAS, 449, 4494
Hoyle F., Vogeley M. S., 2004, ApJ, 607, 751
Ilić S., Langer M., Douspis M., 2013, A&A, 556, A51
Kashlinsky A., Atrio-Barandela F., Kocevski D., Ebeling H., 2008, ApJ, 686, L49

Lambas D. G., Lares M., Ceccarelli L., Ruiz A. N., Paz D. J., Maldonado V. E., Luparello H. E., 2016, MNRAS, 455, L99 (GL16)
Lavaux G., Wandelt B. D., 2010, MNRAS, 403, 1392
Lavaux G., Tully R. B., Mohayaee R., Colombi S., 2010, ApJ, 709, 483
Ma Y.-Z., Pan J., 2014, MNRAS, 437, 1996
Ma Y.-Z., Li M., He P., 2015, A&A, 583, A52
Neyrinck M. C., 2008, MNRAS, 386, 2101
Nusser A., Branchini E., Davis M., 2011, ApJ, 735, 77
Padilla N. D., Ceccarelli L., Lambas D. G., 2005, MNRAS, 363, 977
Pápai P., Szapudi I., Granett B. R., 2011, ApJ, 732, 27
Paz D., Lares M., Ceccarelli L., Padilla N., Lambas D. G., 2013, MNRAS, 436, 3480
Peebles P. J. E., 1980, The Large-scale Structure of the Universe. Princeton Univ. Press, Princeton, NJ
Pivato M. C., Padilla N. D., Lambas D. G., 2006, MNRAS, 373, 1409
Ruiz A. N., Paz D. J., Lares M., Luparello H. E., Ceccarelli L., Lambas D. G., 2015, MNRAS, 448, 1471
Sheth R. K., van de Weygaert R., 2004, MNRAS, 350, 517
Springel V., 2005, MNRAS, 364, 1105
Strauss M. A. et al., 2002, AJ, 124, 1810
Sutter P. M., Lavaux G., Wandelt B. D., Weinberg D. H., 2012, ApJ, 761, 187
Sutter P. M., Elahi P., Falck B., Onions J., Hamaus N., Knebe A., Srisawat C., Schneider A., 2014, MNRAS, 445, 1235
Turnbull S. J., Hudson M. J., Feldman H. A., Hicken M., Kirshner R. P., Watkins R., 2012, MNRAS, 420, 447
Wang H., Mo H. J., Jing Y. P., Guo Y., van den Bosch F. C., Yang X., 2009, MNRAS, 394, 398
Wang H., Mo H. J., Yang X., van den Bosch F. C., 2012, MNRAS, 420, 1809
Watkins R., Feldman H. A., 2015, MNRAS, 447, 132
Watkins R., Feldman H. A., Hudson M. J., 2009, MNRAS, 392, 743
White S. D. M., 1979, MNRAS, 186, 145
Wojtak R., Powell D., Abel T., 2016, MNRAS, 458, 4431

APPENDIX A: THE LINEARIZED PECULIAR VELOCITY FIELD

The analysis of large-scale dynamics is limited by the lack of sufficiently large samples of galaxies with measured peculiar velocities with reasonable accuracy which requires the determination of distances independent of redshift.

For this reason, in order to study the motions of observational voids, we use a reconstructed velocity field using linear theory by Wang et al. (2009, 2012) in the SDSS volume. We have already adopted these linearized velocities to estimate the bulk motions of voids identified in the SDDS in GL16 where we claim a strong alignment and small moduli difference between linearized and fully non-linear velocities. We provide here the details of the analysis of the effects of using linearized velocities to estimate bulk void velocities.

We also showed in GL16 that the shell mean velocity is representative of the velocity of the void core by comparing the velocity obtained from simulated haloes at void walls ($0.8 < r/R_{\rm void} < 1.2$) to the obtained using the mass distribution (particles) in the region $r/R_{\rm void} < 0.8$. Here we show that this result is also valid for observational voids by comparing their core and shell velocities. In the upper panel of Fig. A1 we show an estimate of the density of voids as a function of the angle between the core and the shell velocities (θ) and the difference of the moduli between both velocities obtained from the SDSS+linearized velocity field (shaded contours). In dashed lines we show the same quantity computed for the linearized velocities in the numerical simulation. These velocities where obtained applying the same linear reconstruction procedure to the simulated halo catalogue. As it can be seen, the difference between the velocity directions are smaller than 5°, meanwhile the difference in magnitude is lower than 8 per cent. To quantify the impact of this approximation to the true velocities of void shells, we have implemented the method introduced by Wang et al. (2009) to the density field traced by the massive dark matter haloes in the simulation. Then, we can infer the linear velocity field in the simulation box in a similar fashion than in the observational data. The lower panel of Fig. A1 shows the probability density of voids in the simulation as a function of the angle ϕ and the relative difference between both velocities. By inspection to this figure we can notice that the lineal reconstruction of the velocity field has uncertainties in ϕ typically lower than 15°and 40 per cent in moduli. Taking into account these results, we argue that linear theory provides a suitable approximation to the actual void shell velocities, and therefore can be used to study the motions of observational voids.

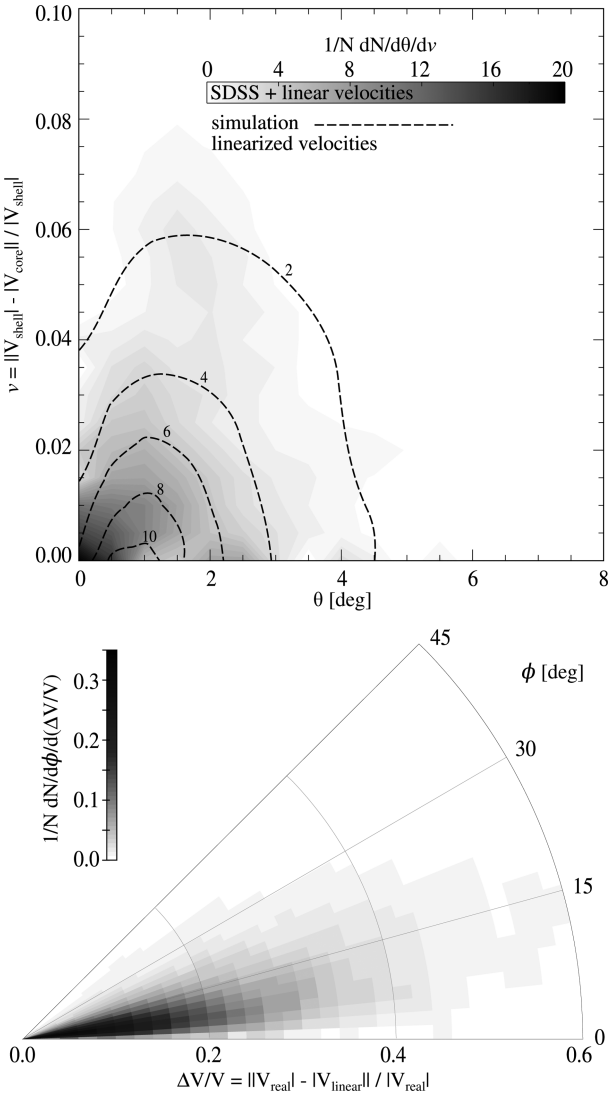

Figure A1. Upper panel: probability density as a function of the angle between the core and shell velocities (θ) and the relative difference between both velocities obtained from the SDSS+linearized velocity field. The dashed lines corresponds to the same quantities computed through the linearized velocities of the simulation. Lower panel: polar diagram of the probability density as a function of the angle ϕ and the relative difference between the full and the linearized velocity estimates of voids.

This paper has been typeset from a TEX/LATEX file prepared by the author.